FOUNTAIN JOURNAL OF NATURAL & APPLIED SCIENCES

A Publication of the College of Natural & Applied Sciences

Fountain University, Osogbo, Nigeria

# Fabrication of tripartite green-synthesised AgNPs/Nanobiochar/Co-MOF composite for adsorptive removal of methylparaben: adsorption, mechanistic and thermodynamic investigations

**Ayinde, Y. T.[1,2*], Azeez, L., Popoola, S. A., Bolarinwa, H. S., Awolola, O.S., Sulaiman, W. K., Oladeji, R. D.**

*[1]Department of Pure and Applied Chemistry, Osun State University, Osogbo, Nigeria.*
*[2]Department of Chemistry, Islamic University of Madinah, Saudi Arabia*
*3 Department of Physics, Electronics and Earth Sciences, Fountain University, Osogbo*
*[4]Department of Chemistry, School of Science, Federal College of Education (Special), Oyo, Nigeria.*

**Correspondence: luqman.azeez@uniosun.edu.ng*

**ABSTRACT**

The tripartite composite of silver nanoparticles (AgNPs), Nanobiochar, and cobalt metal-organic frameworks (Co-MOF) was prepared via a non-thermal, hydro-based method. The successful integration of AgNPs, Nanobiochar, and Co-MOF was ascertained via Fourier Transform Infrared (FTIR) spectroscopy, energy-dispersive X-ray (EDX) spectroscopy, Transmission electron microscopy (TEM), Brunauer–Emmett–Teller (BET) analysis, and molecular docking optimisation. The adsorption process of the AgNPs/Nanobiochar/Co-MOF composite–methylparaben (MPB) was examined experimentally and computationally using Density functional theory (DFT). The pH point of zero charge of the AgNPs/Nanobiochar/Co-MOF composite was observed at 8.8, while maximum adsorption occurred at pH 6. The thermodynamic, isotherm, and kinetic evaluation of the adsorption data indicates that the adsorption process is exothermic and best described by the Freundlich isotherm and pseudo-second-order (PSO) kinetics. The adsorption process of methylparaben (MPB) on the AgNPs/Nanobiochar/Co-MOF composite is characterised as physisorption, exothermic, spontaneous, and multilayered, as revealed by negative values of enthalpy (ΔH°) and free energy (ΔG°), with a monolayer adsorption capacity (qmax) of 45.19 mg $g^{-1}$. The adsorption process, as predicted by Density functional theory (DFT) results, indicates that adsorption arises from interaction of methylparaben (MPB) with the Co metal centre of the composite complex [$CH_3O$---Co or C=O---Co] or the uncoordinated N atom of the imidazole ring [C=O---H-Imz, -N---H-Ph]. The complex [$CH_3O$---Co] is the most probable mode of interaction owing to lower predicted ΔG, greater binding energy, electron transfer, and a possible contribution from hydrogen bonding in complex [C=O---H-Imz, -N---H-Ph] at elevated temperature.

**ARTICLE INFO**

**Article history:**
Received March 2026
Revised April 2026
Accepted April 2026

**Keywords:**
Density functional theory, Metal-organic framework, Nanobiochar, Silver nanoparticles, Methylparaben adsorption
.



## Introduction

Screening water samples for endocrine-disrupting chemicals (EDCs) is pertinent for safeguarding against toxicity and hormonal disruption (1). Many EDCs are released into environmental water samples through runoff from nonpoint sources and effluents from sewage and industrial treatment plants (2). EDCs are a new class of emerging contaminants whose name derives from their interference with the endocrine system, stimulating several pathological disorders in females and males, ranging from reproductive and cancer-related disorders to metabolic dysfunction and neuro-behavioural dysfunctions (3).

An important group of EDCs is parabens. Parabens are alkyl esters of 4-hydroxybenzoic acid;



**DOI:** https://doi.org/10.53704/fujnas.v15i2.1330

the parabens family comprises methyl, ethyl, propyl, and butyl parabens, among others. Parabens are utilised in about 80% of pharmaceuticals and personal care products (PPCPs) (4) to inhibit enzymatic action and impair protein in microbial cells. This has resulted in the distribution of parabens across aquatic ecosystems, including water bodies, soils, the atmosphere, aquatic biota, and human tissues (5). Recently, a myriad of reports have spotlighted the paraben family in numerous toxicological effects such as telomere shortening, endocrine disruption, and thyroid inhibition (4). In humans, parabens have been identified as a cause of breast tumours in females and male infertility (6).

In contrast to other EDC removal techniques, adsorption offers high efficiency, simple operating conditions, an environmentally friendly process, and low operational costs in aqueous media (1). Parabens are detected at sub-$\mu g \cdot L^{-1}$ levels in wastewater and in effluents treated by processes such as ozonation, chlorine dioxide treatment, and photodegradation, as well as in disinfection by-products (6). The adsorption method for removing parabens offers a safer, more eco-friendly alternative. However, the efficiency and feasibility of the adsorption technique depend on the adsorption system design, the choice of adsorbent, the relative abundance of the precursor material, and recyclability (6). According to reports, numerous adsorbents such as carbon nanotubes, mesoporous silica (2), biopolymers, fly ash, nanoparticles (7); (8), activated carbon (9), chitosan (6), microplastics (10), Biochar (11), modified cellulose (12), have been applied in the separation of parabens from aqueous solution. However, most of these adsorbents suffer from low reusability, difficult separation, low adsorption capacity, high cost, and low selectivity (13, 14). Therefore, to overcome this challenge, a suitable adsorbent material with high adsorption capacity and selectivity must be identified and developed for paraben removal.

Lately, metal-organic frameworks (MOFs), porous materials with an infinite periodic structure formed from metal clusters and organic linkers, have numerous advantages over other adsorbents, including easy functionalization, large surface area, high flexibility and porosity, broad selectivity, and uniform pore size (15,16). MOFs have been utilised for hydrogen storage, $CO_2$ capture, drug delivery, and catalysis (17). Zeolitic imidazolate frameworks (ZIFs) are a group of MOF materials synthesised from cobalt or zinc metal precursors and organic ligands (2-methylimidazole). Various zeolitic imidazolate frameworks (ZIFs) have been successfully synthesised for pollutant adsorption, including ZIF-8, ZIF-9, ZIF-10, ZIF-67, ZIF-71, ZIF-76, and ZIF-78 (18). The synthesis of ZIF is mild and easy to perform, yielding a high yield of efficient nanoparticle material for pollutant adsorption. However, ZIFs, like most metal-organic frameworks, have the drawback of being difficult to recover from solution and requiring high-speed centrifugation to effect separation (15, 19).

Based on the above considerations, a tripartite composite comprising a cobalt metal-organic framework, silver nanoparticles (AgNPs), and nano biochar has been fabricated to improve its recyclability and adsorption performance.

In this study, a novel AgNPs/Nanobiochar/Co-MOF composite is fabricated and applied to selectively adsorb methylparaben, an endocrine-disrupting chemical (EDC). This study aims to develop an efficient, cost-effective, recyclable, high-capacity adsorbent material to meet the needs of water treatment systems contaminated with EDCs. Furthermore, the adsorption mode of methylparaben on the AgNPs/Nanobiochar/Co-MOF composite was theoretically demonstrated using density functional theory (DFT) calculations and Molecular docking.

## Experimental

### Materials

Methylparaben, 2-methylimidazole, cobalt nitrate hexahydrate, and silver nitrate salt were all analytical reagent grade purchased from Sigma Aldrich, Germany.

### Synthesis of AgNPs/Nanobiochar/Co-MOF composite

### Synthesis of silver nanoparticles

The synthesis of silver nanoparticles (AgNPs) was mediated as described by Azeez and co-workers (20, 21). Briefly, 1 mL of extract obtained from the boiling of aqueous *Anthocleista nobilis* leaf was added to 40 mL of 1 mM silver nitrate solution, and the reaction was monitored until a stable golden coloured solution was observed.

### Synthesis of Nanobiochar

The Nanobiochar was synthesised using the bark of the Anthocleista nobilis plant, with slight modifications to the method of Wei et al. (22). The bark was washed with water, dried under ambient conditions for 7 days, pulverised, and sieved to a



DOI: https://doi.org/10.53704/fujnas.v15i2.1330

uniform size. The pulverised bark was pyrolysed in a muffle furnace (Witeg, FHP muffle furnace) under limited oxygen conditions at a temperature of 400 °C for 2 h. The pyrolysis product was granulated and passed through a 45 µm sieve to obtain fine biochar powder (Standard test sieve (IS-460)).

**Synthesis of Co-MOF**

The Co-MOF was synthesised according to the method of Al Murisi and co-workers (23). Cobalt nitrate hexahydrate (0.582 g or 2 mmol) and 2-methylimidazole (1.323 g or 16 mmol) were dissolved in separate containers with 40 mL of deionised water, respectively. The methylimidazole solution was added to the cobalt nitrate solution, and the mixture was stirred at 300 rpm for 6 h at room temperature. The precipitate formed was separated by centrifuging at 8000 rpm for 30 min under normal room conditions, washed three 3 times with deionised-distilled water, and dried at 70 °C overnight.

**Synthesis of AgNPs/Nanobiochar/Co-MOF composite**

The silver nanoparticles and nano biochar were integrated into the cobalt metal-organic framework (Co-MOF) using a method described by (24, 25). Precisely, 1.28 g of 2-methylimidazole (2-MIM) and 0.87 g of cobalt nitrate hexahydrate ($Co(NO_3)_2 \bullet 6H_2O$) were dissolved separately in 30 ml of deionised water, followed by dispersion of 0.21 g of silver nanoparticles (AgNPs) and Nanobiochar in the cobalt solution. The resulting solution was stirred for 2 h to ensure homogeneity. Afterwards, the 2-MIM solution was added dropwise to the previous solution, and the mixture was stirred continuously at 300 rpm under room conditions for 7 h. The purple-coloured solid composite material was separated from the solution by centrifugation at 8000 rpm for 30 min under normal room conditions, washed with a mixture of ethanol/water (1:2), and dried overnight at 80 °C.

**Characterisation**

UV–Visible spectroscopy was used to characterize the green synthesized AgNPs by scanning from 190 to 900 nm for the characteristic peak in a Biobase BK-UV1900 PC spectrometer, Fourier Transform Infra-Red spectroscopy (FTIR) was used to determine functional groups present in AgNPs/Nanobiochar/Co-MOF composite and constituting material in a Shimadzu FTIR 8400S spectrometer, The pore size distribution, surface elemental and morphological composition of AgNPs/Nanobiochar/Co-MOF composite and constituting material were analyzed using Quantachrome Autosorb 1 series Brunauer-Emmett-Teller (BET), energy dispersive X-ray (EDX, TESCAN VEGA 3 LMH) and Transmission electron microscopy (TEM, HT7830).

**pH point of zero charge ($pH_{pzc}$)**

The pH point of zero charge ($pH_{pzc}$) of 0.5 g of AgNPs/Nanobiochar/Co-MOF composite in 25mL of 0.1 M NaCl was determined using a pH-3C HELLONG pH meter and recorded as the initial pH. The final pH values were obtained by varying the initial pH from 1 to 12 with 0.1 M HCl/NaOH and were determined after 24 h. The point of zero charge of the composite was taken as the y-axis intercept from the plot of change in pH (ΔpH) against initial pH (26).

**Batch adsorption experiment**

A stock solution of Methylparaben (MPB) was prepared by adding 100 mg of triclosan to 100 mL of methanol. The sample solutions were prepared by diluting the stock solution with 20% methanol in deionised/distilled water. The optimum pH for MPB removal from solution was investigated by varying the pH of the MPB solution from 2 to 12, with a composite dose of 0.3 g, a temperature of 303 K, an agitation speed of 150 rpm, and a concentration of 50 mg $L^{-1}$. The influence of composite dose was determined by varying the adsorbent dosage from 0.1 to 0.5 g in 0.1 g increments, with a fixed contact time of 30 min, a concentration of 50 mg L-1, pH 6, 303 K, and an agitation speed of 150 rpm. The effect of initial concentration on the percentage of methylparaben adsorbed from solution was determined by varying the MPB concentration from 10 to 70 mg L-1, with a fixed adsorbent dosage of 0.5 g, a temperature of 303 K, a pH of 6, an agitation speed of 150 rpm, and a contact time of 30 min. The time of adsorption and the effect of temperature on the adsorption process of methylparaben was varied from 5 to 100 min at 5 min interval and 303 to 313 K using the optimum condition obtained from the study of effect of pH, adsorbent dose and initial MPB concentration; after adsorption, the composite was separated from methylparaben solution through centrifugation at 7000 rpm, the absorbance of MPB at equilibrium was measured at 290 nm with a UV-visible spectrophotometer (BK-UV1900 PC, China) and interpolated to concentration.



DOI: https://doi.org/10.53704/fujnas.v15i2.1330

The percentage removal and the quantity of methylparaben (MPB) adsorbed per gram of composite were evaluated using equations 1 and 2 below.

$$\% R = \left(\frac{C_o - C_e}{C_o}\right) x\ 100 \quad (1)$$

$$q_e = \frac{V}{m}\ (C_0 - C_e) \quad (2)$$

where $q_e$ (mg $g^{-1}$) is the quantity of compound adsorbed per mass unit of composite, $C_o$ (mg $L^{-1}$) is the initial MPB concentration, $C_e$ (mg $L^{-1}$) is the residual equilibrium MPB concentration, V (L) is the volume of MPB solution, and m is the quantity of AgNPs/Nanobiochar/Co-MOF composite (g).

**Adsorption models**

**Adsorption isotherm**

The data obtained from the adsorption study were used to evaluate the adsorption process. The data were fitted to the equations corresponding to four adsorption isotherm models: Langmuir (3 and 4), Freundlich (5), Temkin (6a and 6b) and Dubinin-Radushkevich (7a, 7b and 7c). Where $C_e$ and $q_e$ represent methylparaben equilibrium concentration (mg$L^{-1}$) and quantity adsorbed per unit mass (mg $g^{-1}$), $q_{max}$ and $K_L$ represent maximum monolayer adsorption of AgNPs/Nanobiochar/Co-MOF composite and Langmuir isotherm correlated to the energy of adsorption. n and $K_f$ correspond to the heterogeneity factor and the favourability constant of the Freundlich isotherm model. Where b (J/mol) represents the Temkin heat of adsorption, and A represent the equilibrium binding constant. β, ε and E (kJ/mol) in Dubinin–Radushkevich equations represent the constant related to free energy, Polanyi potential and the adsorption energy.

$$\frac{Ce}{q_e} = \frac{Ce}{q_{max}} + \frac{1}{q_{max} K_L} \quad (3)$$

$$R_L = \frac{1}{1 + K_L C_o} \quad (4)$$

$$Log\ q_e = \frac{1}{n}\ Log c_e + Log\ K_F \quad (5)$$

$$q_e = B ln A + B ln C_e \quad (6a)$$

$$B = \frac{RT}{b} \quad (6b)$$

$$ln q_e = ln q_o - \beta \epsilon^2 \quad (7a)$$

$$\epsilon = RT ln\left(1 + \frac{1}{C_e}\right) \quad (7b)$$

$$E = \sqrt{\frac{1}{2\beta}} \quad (7c)$$

**Adsorption kinetics**

The data were fitted to the equations corresponding to four adsorption kinetics models (Pseudo first-order (8), pseudo second-order (9), Elovich (10) and Intra-particle diffusion (11). Where $q_t$ in adsorption kinetic equations (8 – 11) corresponds to the quantity of methylparaben adsorbed per unit time (mg $g^{-1}$), while $K_1$ and $K_2$ correspond to the rate constant of pseudo-first and pseudo-second order kinetic models. α and β in the Elovich equation represent the initial adsorption rate constant (mg $g^{-1}$ $min^{-1}$) and the desorption constant related to the chemisorption activation energy and the surface coverage (g $mg^{-1}$), qt is the adsorbed dye (mg $g^{-1}$) at time t (min). $K_{diff}$ is the kinetic model's intraparticle diffusion rate constant (mg $g^{-1}$ $min^{-1/2}$), and C is the constant which provides the film thickness between the adsorbate and the adsorbent.

$$\ln(q_e - q_t) = \ln q_e - k_1\ t \quad (8)$$

$$\frac{t}{q_t} = \frac{1}{k_2\ qe^2} + \frac{1}{q_e}\ t \quad (9)$$

$$q_t = \frac{1}{\beta}\ln(\alpha\beta) + \frac{1}{\beta}\ lnt \quad (10)$$

$$q_t = K_{diff} t^{\frac{1}{2}} + C \quad (11)$$

**Adsorption thermodynamics**

The thermodynamic parameters were calculated from equations 12 and 13. R, T, $G^o$, $H^o$, and $S^o$ . Equations 12 and 13 correspond to the universal gas constant (8.314 $Jmol^{-1}K^{-1}$), temperature (K), free energy change, enthalpy change, and entropy change. The best model was determined using the root mean square error (RMSE; Equation (14)).

$$lnK_c = \frac{\Delta S}{R} - \frac{\Delta H}{R}\left(\frac{1}{T}\right) \quad (12)$$

$$\Delta G^o = \Delta H^o - T\Delta S^o \quad (13)$$

$$RMSE = \sqrt{\frac{1}{n-1}\sum_{i-1}^{n}\left(q_{e,means} - q_{e,cal}\right)^2} \quad (14)$$

**Molecular docking study**

**Quantum chemical elucidation of methylparaben (MPB) adsorption by AgNPs/Nanobiochar/Co-MOF composite**

To annotate the alliance of methylparaben (MPB) with AgNPs/Nanobiochar/Co-MOF composite, the structures of the AgNPs/Nanobiochar/Co-MOF composite and MPB were optimised without geometrical constraint, utilising Gaussian 16 software (Frisch and Trucks 2016) (27). The electronic properties of methylparaben (MPB) liable for interfacing with the composite and molecular orbital (HOMO and LUMO) electron density of MPB were determined by density functional theory (DFT) approach using B3LYP methods (46, 47) with def2svp as the basis set (28, 29) and inclusion of empirical dispersion gd3 to account for the non-covalent interactions (45). Following the optimisation, a



DOI: https://doi.org/10.53704/fujnas.v15i2.1330

frequency calculation was conducted to assess the nature of convergence, and all wavenumbers were found to be real. The Frontier molecular orbitals and molecular electrostatic potential surfaces were generated from the checkpoint file, while the reactivity parameters were computed using methods reported in the literature (44). Moreover, the choice of the basic set was based on its ability to give results that agree with the experimental data (28, 29).

## Results and discussion

### Characterisation of AgNPs/Nanobiochar/Co-MOF composite

The silver nanoparticle-mediated *Anthocleista nobilis* leaf extract was golden in colour and absorbed maximally ($\lambda_{max}$) at 325 nm with a broad plasmonic peak (Fig. 1).

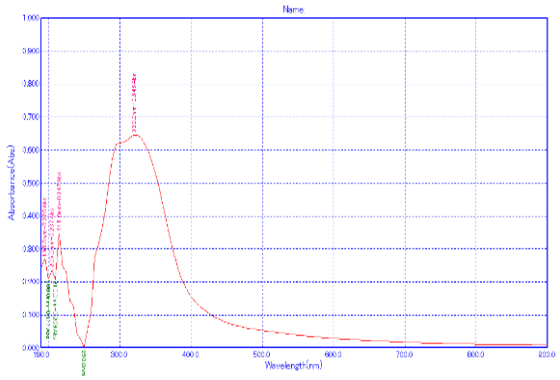


**Figure 1. UV–visible spectrum absorption of *Anthocleista nobilis* leaf extract mediated AgNPs**

The peak of silver nanoparticle mediated with *Anthocleista nobilis* leaf extract obtained from this study lies within the characteristic range of AgNPs (21, 26). The biomolecules liable for limiting, reducing, and stabilizing $Ag^{+}$ to $Ag^{0}$ in the leaf extract of *Anthocleista nobilis* are revealed in the FTIR spectra of silver nanoparticles AgNPs (Fig. 2). The spectra showed peaks that are characteristic of O-H stretch, C=C, and bending OH of phenols at 3414,1636, and 1385 $cm^{-1}$, implying that polyphenols are liable for the capping and stabilizing of silver nanoparticles (21, 26, 30).

Prominent peaks such as N-H, Co-N in spectra of Co-MOF, OH peak in spectra of AgNPs, and Nanobiochar were evident in the spectra of AgNPs/Nanobiochar/Co-MOF composite, which indicates the successful synthesis of the composite. The FTIR spectra (Fig. 3) of Nanobiochar synthesised from *Anthocleista nobilis* bark showed bands at 3421, 1556, 1165, and 1060 $cm^{-1}$ corresponding to stretching of O-H (in carboxyl, phenol, or alcohol unctional groups), C=O of carboxylic acid, and C-O of alcohol, respectively. The existence of a broad hydroxyl (O-H) group and a well-developed aromatic backbone, evidenced by sharp peaks at 1566 and 1427 cm–1 in the FTIR spectrum of the Nanobiochar, indicates a high density of oxygen-containing functional groups with significant reactivity and hydrophilicity (20, 30, 31).

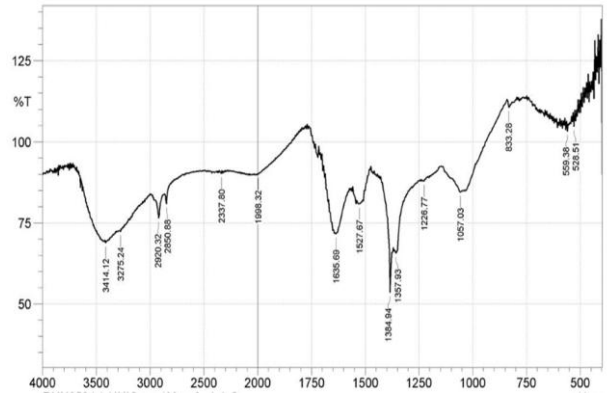


**Figure 2. Fourier transform infrared (FT-IR) spectrum of *Anthocleista nobilis* leaf mediated AgNPs**

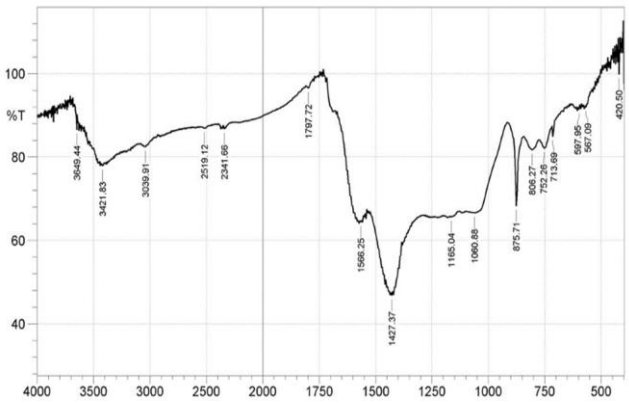


**Figure 3. Fourier transform infrared (FT-IR) spectrum of Nanobiochar produced from Anthocleista nobilis bark**

The FTIR spectra (Fig. 4) of Co-MOF showed bands between 3167 and 2920 $cm^{-1}$ attributable to stretching modes of N-H in 2-methylimidazole. The peaks at 1566, 1415, and 1384 $cm^{-1}$ correspond to C=N, C=C, and C-N vibrations in the 2-methylimidazole ring. The sharp peak observed at 429 $cm^{-1}$ corresponds to the Co-N bond. This confirms the successful synthesis of Co-MOF (25, 32). The FTIR spectra (Fig. 5) of AgNPs/Nanobiochar/Co-MOF composite showed peaks 3398, 1384, 1141, 1562, 1419, and 428 $cm^{-1}$ corresponding to O-H or N-H stretching, bending of O-H of phenols or C-N stretching in 2-methylimidazole, C-O of alcohol, C=O of carboxylic acid, C=C in 2-methylimidazole, and Co-N bond in Co-MOF. The high-intensity peak at



DOI: https://doi.org/10.53704/fujnas.v15i2.1330

428 $cm^{-1}$, the preservation of the imidazole ring, and the enhancement of the peak at 1384 cm–1 suggest the synergistic overlap between the methyl group of the ligand and the capping agent of the nanoparticles, and the successful immobilisation of Co-MOF on Nanobiochar and nanoparticles.

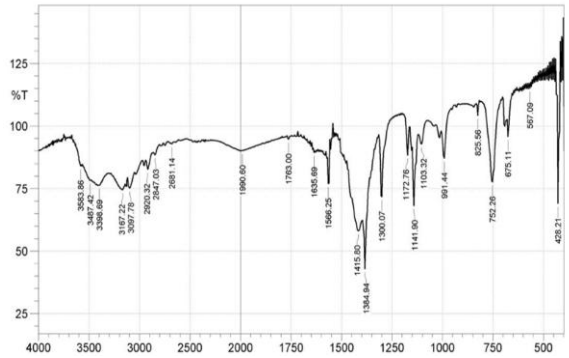


**Figure 4. Fourier transform infrared (FT-IR) spectrum of Co-Metal organic framework (Co-MOF)**

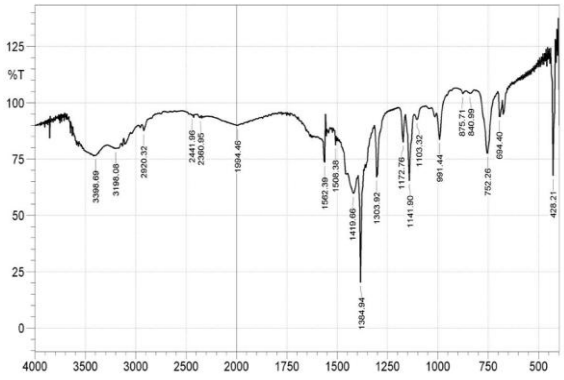


**Figure 5. Fourier transform infrared (FT-IR) spectrum of AgNPs/Nanobiochar/Co-MOF composite**

The TEM micrograph of Co-MOF (Fig. 6) showed particles with a definite facet and an average particle size of 21.11 nm. The synthesised Co-MOF exhibited a similar characteristic rhombic dodecahedral morphology to most reported Co-MOFs (24). The shapes of the Nanobiochar, nanoparticle, and AgNPs/Nanobiochar/Co-MOF composite (Fig. 7, 8 and 9). ranged from oval to round, with average particle sizes of 28.51, 14.15, and 15.0 nm for Nanobiochar, nanoparticles, and composite, respectively. The EDX spectra (Fig. 11, 12, 13 and 14) of Co-MOF, Nanobiochar, nanoparticle, and AgNPs/Nanobiochar/Co-MOF composite displayed Co (53.85 %), N (20.58 %), and O (13.72 %) in Co-MOF, Si (50.98 %), C (5.18 %), and O (10.68 %) in Nanobiochar, Ag (54.79 %) in silver nanoparticle, and Si (40.35 %), Ag (20.30 %), Co (7.32 %), C (3.2 %) in composite.

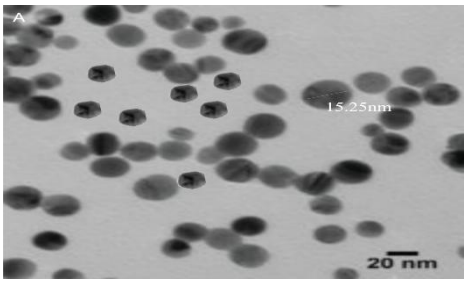


**Figure 6. Transmission electron micrographs (TEM) of Co-metal organic framework (Co-MOF)**

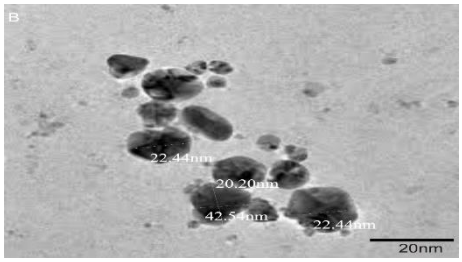


**Figure 7. Transmission electron micrographs (TEM) of Nanobiochar produced from *Anthocleista nobilis***

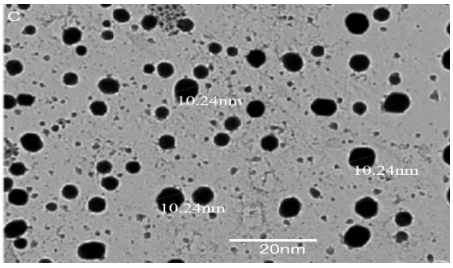


**Figure 8. Transmission electron micrograph (TEM) of *Anthocleista nobilis* leaf mediated AgNPs**

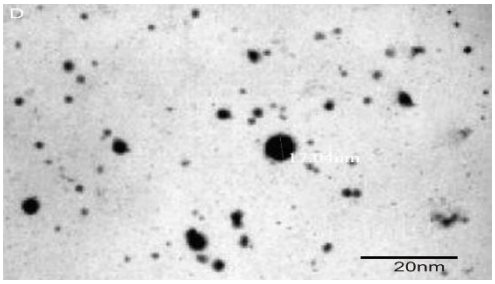


**Figure 9. Transmission electron micrograph (TEM) of AgNPs/Nanobiochar/Co-MOF composite**

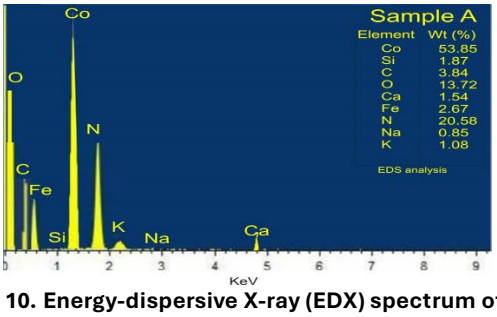


**Figure 10. Energy-dispersive X-ray (EDX) spectrum of Co-Metal organic framework (Co-MOF)**



**DOI:** https://doi.org/10.53704/fujnas.v15i2.1330

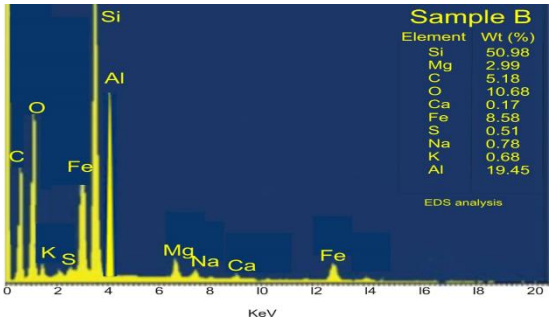


**Figure 11. Energy-dispersive X-ray (EDX) spectrum of Nanobiochar produced from *Anthocleista nobilis* bark**

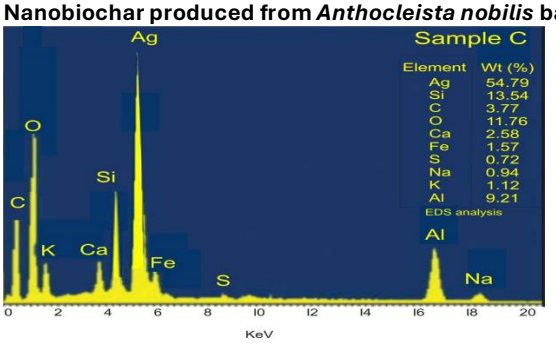


**Figure 12. Energy-dispersive X-ray (EDX) spectrum of *Anthocleista nobilis* leaf mediated AgNPs**

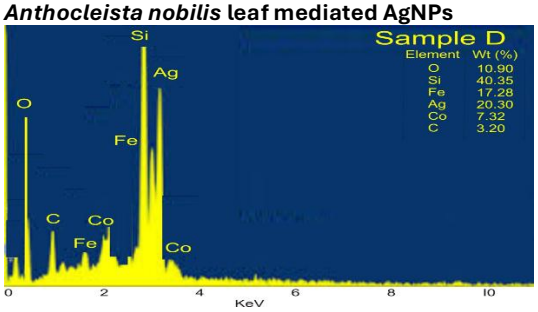


**Figure 13. Energy-dispersive X-ray (EDX) Spectrum of AgNPs/Nanobiochar/Co-MOF composite**

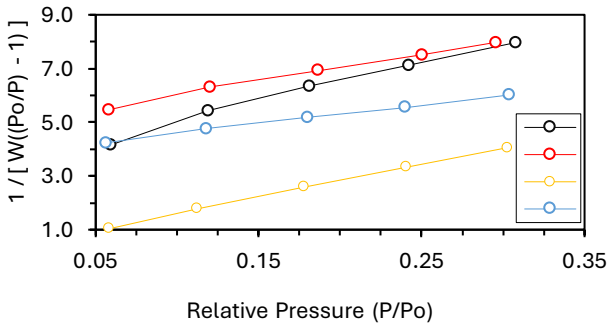


**Figure 14. $N_2$ adsorption for the isotherm for Co-MOF (A), Nanobiochar (B), AgNPs (C) and AgNPs/Nanobiochar/Co-MOF composite (D).**

The BET characterization of Co-MOF (A), Nanobiochar (B), AgNPs (C), and AgNPs/Nanobiochar/Co-MOF composite (D) at 77 K (Fig. 14). Nanobiochar (B), AgNPs (C), and AgNPs/Nanobiochar/Co-MOF composite (D) exhibited textural properties of a type I isotherm and a $N_2$ adsorption–desorption (Fig. 15, 16, 17 and 18) cycle with a H4 hysteresis loop, except Co-MOF (A), which showed a type IV isotherm. The results showed that Surface area (SBET), total volume, average pore diameter, and micropore surface area (Table 1) indicate that the composite and the constituting material comprise mesoporous cavities, as the pore diameters lie within the range of 2 – 50 nm (33). The BET surface area measured for AgNPs/Nanobiochar/Co-MOF composite and Co-MOF were 318.3 and 188.5 $m^2$ $g^{-1,}$ respectively. This indicates the harmonious integration of the three components and the provision of additional adsorption sites. The higher total pore volume reported for the composite confirms the enhanced pore accessibility and mesoporous capacity (34). The composite exhibits a larger surface area, greater pore volume and balanced micro-mesoporous features, indicating the synergistic combination of components, which is expected to enhance the removal of adsorbate.

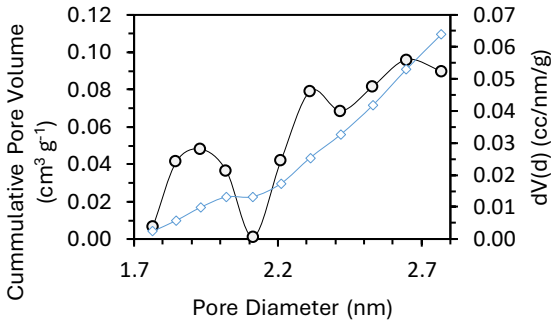


**Figure 15. Pore size distribution for Co-MOF**

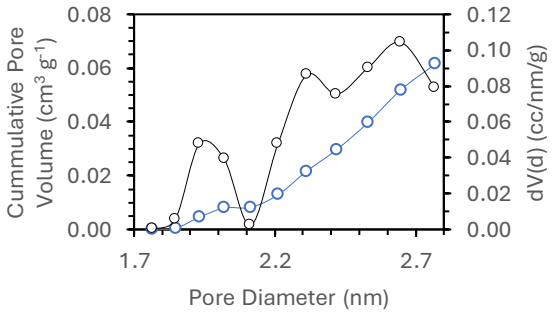


**Figure 16. Pore size distribution for Nanobiochar**

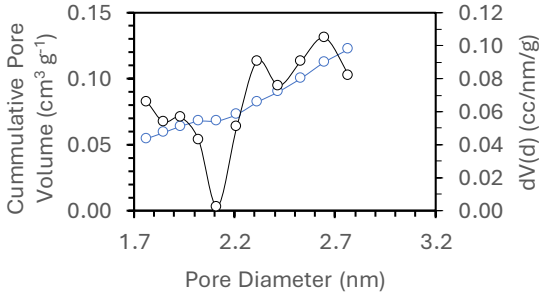


**Figure 17. Pore size distribution for AgNPs**



DOI: https://doi.org/10.53704/fujnas.v15i2.1330

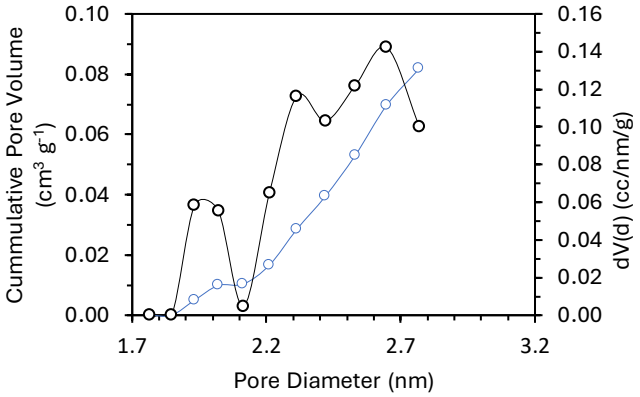


**Figure 18. Pore size distribution for AgNPs/Nanobiochar/Co-MOF composite**

### pH point of zero charge ($pH_{pzc}$)

The point of zero charge ($pH_{pzc}$) of an adsorbent indicates the point (pH) at which the surface of the adsorbent is neutral or charged (7, 10). The point of zero charge of the nanocomposite was observed at a pH of 8.8 (Fig. 19). At this point, the surface of the nanocomposite exhibits neutrality. In contrast, the nanocomposite surface would be positively charged at pH < 8.8 and negatively charged at pH > 8.8. At pH > $pH_{pzc}$, the composite surface was negatively charged and would attract cationic adsorbates; below the $pH_{pzc}$, the composite would be attracted to anionic species.

**Table 1:** Porous structure properties of Co-MOF, Nanobiochar, AgNPs and AgNPs/Nanobiochar/Co-MOF composite

| | Co-MOF | Nanobiochar | Silver NPs | Composite |
|---|---|---|---|---|
| BET surface area ($m^2\ g^{-1}$) | 188.5 | 228.1 | 275.8 | 318.3 |
| Micropore surface area ($m^2\ g^{-1}$) | 228.4 | 234.3 | 393.4 | 315.4 |
| BJH total pore volume (cc $g^{-1}$) | 0.1135 | 0.1168 | 0.1348 | 0.1622 |
| BJH average pore diameter (nm) | 2.647 | 2.153 | 2.108 | 2.133 |

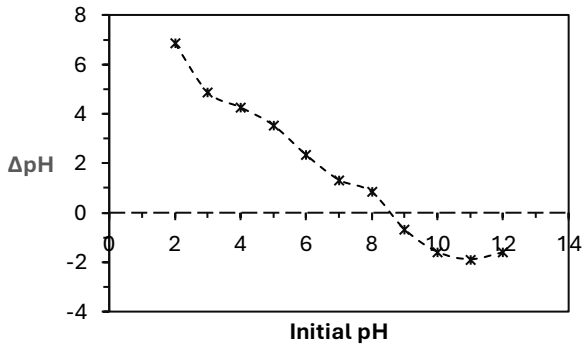


**Figure 19. pH Point of zero charge ($pH_{pzc}$) of AgNPs/Nanobiochar/Co-MOF composite**

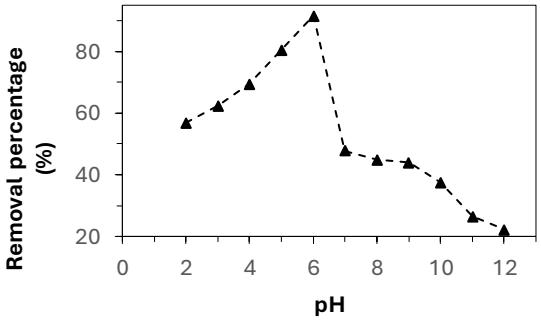


**Figure 20. Effect of pH on removal of methylparaben (MPB) by AgNPs/Nanobiochar/Co-MOF composite (Volume = 25 ml, dose = 0.3 g, Temperature = 303 K, pH = 1 – 12, agitation speed = 150 rpm, time of agitation = 30 min and concentration = 50 mg $L^{-1}$).**

### Influence of operating parameters on methylparaben (MPB) adsorption

The study of adsorption of MPB with respect to pH (Fig. 20) exhibited the highest removal percentage of 91.66 % at pH 6 in experiments with a 0.5 g dose of composite and an initial MPB concentration of 50 m $gL^{-1}$. This aligns with the highest adsorption percentage at pH 6 reported for MPB removal using biochar-$CoFe_2O_4$ nanocomposite by Fito and Nkambule (35). Contrarily, the low removal percentages observed below and above the pH of maximum adsorption (pH 6) are attributable to the ionic state of methylparaben (MPB) and the surface charge of the composite. Methylparaben (MPB) has a pKa value of 8.17; at pH < pKa, methylparaben exists as a neutral molecule, while the ionic form predominates at pH > pKa (6, 10). The percentage uptake increased from pH 2 to 6 due to the attraction between the positively charged surface of the composite and the paraben molecule. The low percentage uptake from pH 6 – 12 declines due to the repulsive force between the composite and anionic MPB. Similar findings were reported by Nodeh et al. (5), Mashile et al. (6), and León et al. (36) regarding the pH



DOI: https://doi.org/10.53704/fujnas.v15i2.1330

at which MPB adsorption is maximal, which occurs on the acidic side of the pH scale.

The significance of composite dose on the adsorption of MPB (Fig. 21) indicates a dose-dependent increase in MPB removal. The removal percentage of MPB increased from 40.17% to a maximum of 90.38% as the composite dose increased from 0.1 to 0.5 g in 25 ml of methylparaben solution. The increase in MPB removal percentage with increasing composite dose is due to an increase in surface and pore sites (5, 8, 10).

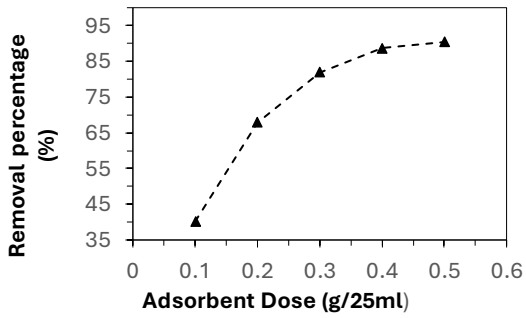


**Figure 21. Effect of AgNPs/Nanobiochar/Co-MOF composite dose on removal of methylparaben (MPB) (Volume = 25 ml, dose = 0.1 – 0.5 g, Temperature = 303 K, pH = 6, agitation speed = 150 rpm, time of agitation = 30 min and concentration = 50 mg $L^{-1}$).**

The correlation between initial MPB concentration (Fig. 22) at pH = 6, 0.5 g of composite, concentration range of 10 – 50 mg $L^{-1}$ and temperature range of 303 – 313 K. The uptake efficiency exhibits an inverse relationship, whereby the removal percentage decreases with increasing temperature and concentration. The high uptake efficiency recorded at low initial concentration is attributed to the presence of superfluous adsorption sites, and the low adsorption efficiency recorded at higher concentration is due to the saturation of adsorption sites (10, 36).

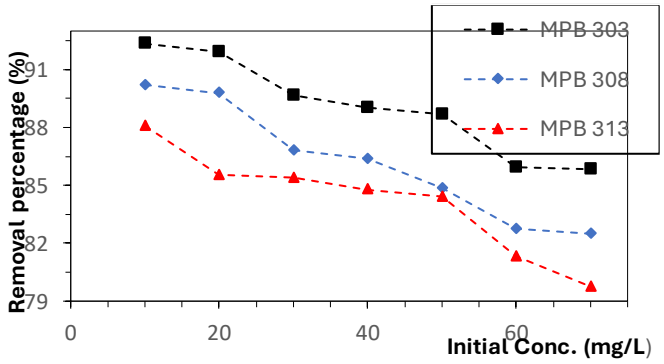


**Fig. 22. Effect of initial methylparaben (MPB) concentration at different temperatures on removal by AgNPs/Nanobiochar/Co-MOF composite (Volume = 25 ml, dose = 0.5 g, Temperature = 303 K, pH = 6, agitation speed = 150 rpm, time of agitation = 30 min and concentration = 10 – 70 mg $L^{-1}$).**

The removal of MPB by AgNPs/Nanobiochar/Co-MOF composite was studied for 100 min. The quantity of methylparaben removed increased from 1.71 mg/g at 5 min to 3.03 mg/g at 70 min, then remained constant. The observed progression indicates that adsorption was rapid until equilibrium between methylparaben and the composite was reached; the contact time necessary to reach the equilibrium between composite and MPB was 70 min (Fig. 23). This is ascribed to the number of vacant sites available for adsorption during the study's early stage, which became fewer as adsorption progressed.

The influence of temperature on the adsorption of MPB was studied between 303 - 333 K at pH = 6, 0.5 g of composite, initial MPB concentration 70 $mgL^{-1}$ (Fig. 24). The adsorption efficiency declined with temperature, indicating that the process of adsorption of MPB by AgNPs/Nanobiochar/Co-MOF composite was exothermic.

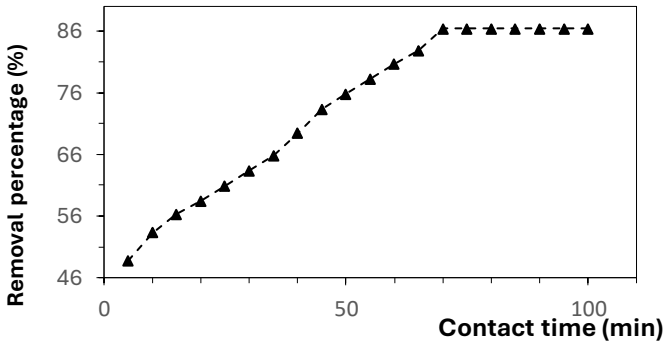


**Figure 23. Effect of contact time on adsorption of methylparaben (MPB) by AgNPs/Nanobiochar/Co-MOF composite (Volume = 25 ml, dose = 0.5 g, Temperature = 303 K, pH = 6, agitation speed = 150 rpm, time of agitation = 5 – 100 min and concentration = 70 mg $L^{-1}$).**

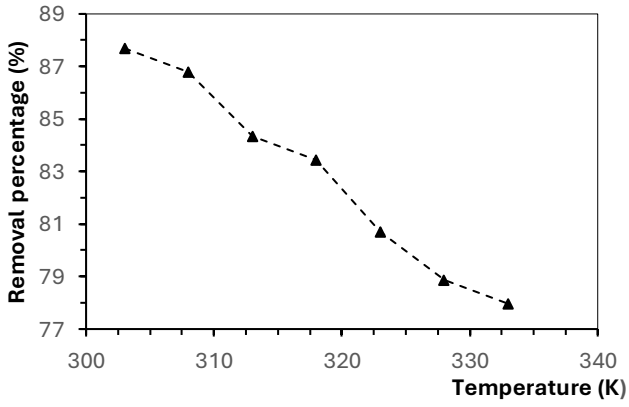


**Figure 24. Effect of temperature variation on adsorption of MPB by AgNPs/Nanobiochar/Co-MOF composite (Volume = 25 ml, dose = 0.5 g, Temperature = 303 K, pH = 6, agitation speed = 150 rpm, time of agitation = 30 min and concentration = 70 mg $L^{-1}$).**



DOI: https://doi.org/10.53704/fujnas.v15i2.1330

## Adsorption isotherm

The adsorption process was modelled using the single-equilibrium adsorption models: Langmuir, Freundlich, Temkin, and Dubinin-Radushkevich. The favourability of the adsorption process, adsorption capacity, and energy requirement of MPB adsorption on the AgNPs/Nanobiochar/Co-MOF composite were obtained from the adsorption isotherms. The plots of the Langmuir and the Freundlich isotherms at different temperatures are shown in Figs. 25 and 26, respectively, and the Temkin and the Dubinin-Radushkevich isotherms are shown in Fig. 27 and 28, respectively, while the resulting parameters from these models are presented in Table 2. The fitness of the adsorption of MPB on AgNPs/Nanobiochar/Co-MOF composite to the models used is determined by the correlation coefficient ($R^2$) and RMSE. The order of fitness of models for MPB was Freundlich ($R^2$ = 0.991, RMSE = 0.441) > Langmuir ($R^2$ = 0.968, RMSE = 1.696) > Temkin ($R^2$ = 0.957, RMSE = 0.208) > Dubinin-Radushkevich ($R^2$ = 0.858, RMSE = 0.511) 303 K, Freundlich ($R^2$ = 0.993, RMSE = 0.376) > Langmuir ($R^2$ = 0.936, RMSE = 1.217) > Temkin ($R^2$ = 0.933, RMSE = 0.248) > Dubinin-Radushkevich ($R^2$ = 0.852, RMSE = 0.506) at 308 K, Freundlich ($R^2$ = 0.990, RMSE = 0.790) > Langmuir ($R^2$ = 0.957, RMSE = 0.794) > Temkin ($R^2$ = 0.936, RMSE = 0.237) > Dubinin-Radushkevich ($R^2$ = 0.809, RMSE = 0.518) at 313 K, Freundlich and Temkin isotherm models best describes the adsorption process of MPB on AgNPs/Nanobiochar/Co-MOF composite as the highest $R^2$ value and the lowest RMSE was recorded for Freundlich and Temkin at all temperatures. This is consistent with the model fit for MPB removal described by the Freundlich isotherm reported by Fito and Nkambule (35).

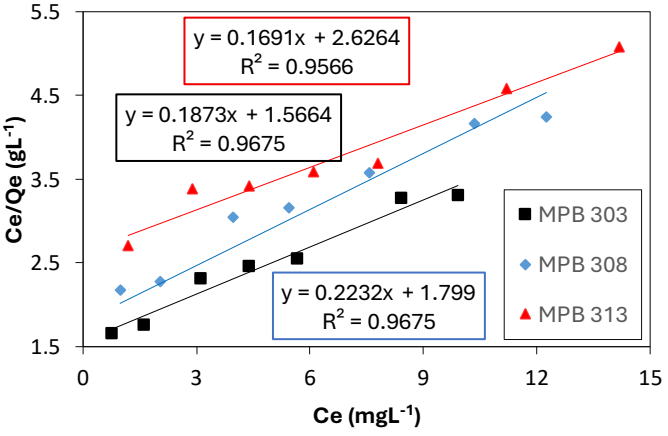


**Figure 25. Langmuir isotherm model of methylparaben (MPB) adsorption on AgNPs/Nanobiochar/Co-MOF composite. (Volume = 25 ml, dose = 0.5 g, Temperature = 303 K, pH = 6, agitation speed = 150 rpm, time of agitation = 30 min and concentration = 10 – 70 mgL⁻¹).**

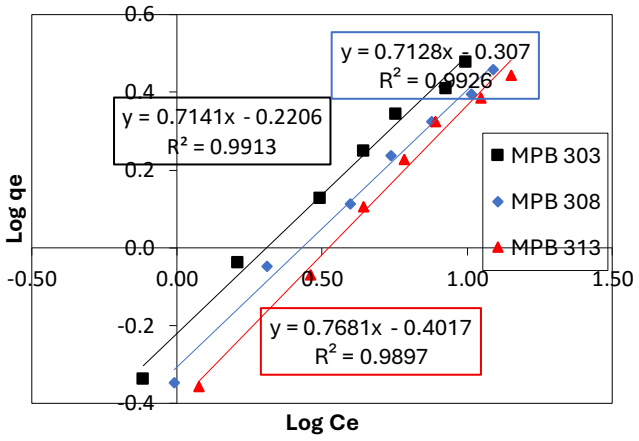


**Figure 26. Freundlich isotherm model of methylparaben (MPB) adsorption on AgNPs/Nanobiochar/Co-MOF composite (Volume = 25 ml, dose = 0.5 g, Temperature = 303 K, pH = 6, agitation speed = 150 rpm, time of agitation = 30 min and concentration = 10 – 70 mgL⁻¹).**

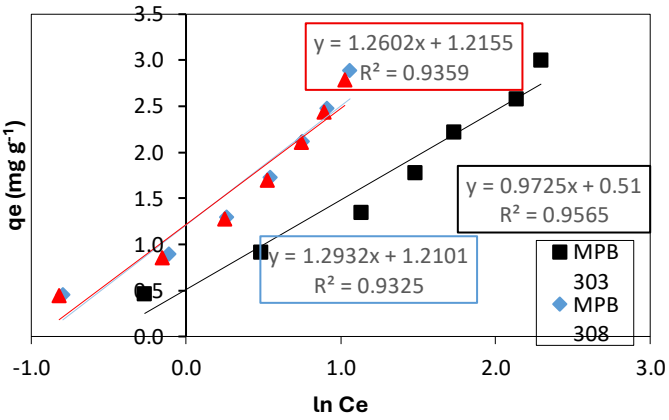


**Figure 27. Temkin isotherm model of methylparaben (MPB) adsorption on AgNPs/Nanobiochar/Co-MOF composite (Volume = 25 ml, dose = 0.5 g, Temperature = 303 K, pH = 6, agitation speed = 150 rpm, time of agitation = 30 min and concentration = 10 – 70 mgL⁻¹).**

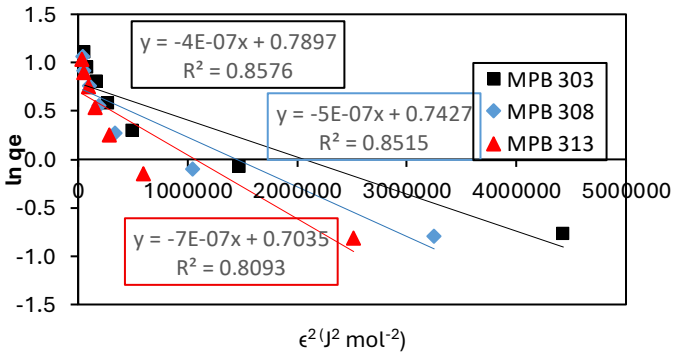


**Figure 28. Dubinin-Radushkevich isotherm model of methylparaben (MPB) adsorption on AgNPs/Nanobiochar/Co-MOF composite (Volume = 25 ml, dose = 0.5 g, Temperature = 303 K, pH = 6, agitation speed = 150 rpm, time of agitation = 30 min and concentration = 10 – 70 mgL⁻¹).**



DOI: https://doi.org/10.53704/fujnas.v15i2.1330

**Table 2: Adsorption isotherm model parameters for methylparaben (MPB) removal by the composite at different temperatures**

| Isotherms | Parameters | Methylparaben | | |
|---|---|---|---|---|
| | | 303 K | 308 K | 313 K |
| Langmuir | $q_{max}$ (mg $g^{-1}$) | 45.19 | 23.90 | 16.84 |
| | $K_L$ (L/mg) | 0.014 | 0.020 | 0.023 |
| | $R_L$ | 0.50 | 0.42 | 0.38 |
| | $R^2$ | 0.968 | 0.936 | 0.957 |
| | *RMSE* | 1.696 | 1.217 | 0.794 |
| Freundlich | n | 1.07 | 1.13 | 1.76 |
| | $K_F$ [L/$mg^{-1}$] | 0.80 | 0.74 | 0.67 |
| | $R^2$ | 0.991 | 0.993 | 0.990 |
| | *RMSE* | 0.441 | 0.376 | 0.790 |
| Temkin | B | 0.9725 | 1.2932 | 1.2602 |
| | A ($Lg^{-1}$) | 1.689 | 2.549 | 2.624 |
| | b ($Jmol^{-1}$) | 2590.4 | 1980.1 | 2065.0 |
| | $R^2$ | 0.957 | 0.933 | 0.936 |
| | *RMSE* | 0.208 | 0.248 | 0.237 |
| Dubinin Radushkevich | $q_o$ ($mgg^{-1}$) | 2.203 | 2.102 | 2.021 |
| | β ($mol^2kJ^{-2}$) | 4E-07 | 5E-07 | 7E-07 |
| | E ($kJmol^{-1}$) | 1.118 | 1.000 | 0.845 |
| | $R^2$ | 0.858 | 0.852 | 0.809 |
| | *RMSE* | 0.511 | 0.506 | 0.518 |

According to the Langmuir isotherm model, the maximum monolayer adsorption capacities ($q_{max}$) at 303, 308, and 313 K for MPB are 45.19, 23.90, and 16.84 mg $g^{-1}$, respectively. The values of $R_L$ in Langmuir isotherm model lie between 0 and 1, while the value of n in the Freundlich isotherm model is greater than 1 (i.e., 0 < RL < 1; n > 1) (Table 2). This indicates that the adsorption process was favourable according to both the Langmuir and the Freundlich models (12). However, the Freundlich model is a better model for adsorption due to the greater correlation coefficient ($R^2$) and lower RMSE value. Higher adsorption capacity was recorded at low temperatures, while lower adsorption capacity was observed at high temperatures. This observation is consistent with the report of Yusoff et al. (37), which found that maximum monolayer adsorption ($q_{max}$) for parabens decreased with temperature. The ($q_{max}$) obtained from the Langmuir plot showed that the AgNPs/Nanobiochar/Co-MOF composite has comparable performance to other previously reported adsorbents for removing MPB (Table 3). According to Freundlich, KF represents the affinity of the composite for MPB; its value decreases with increasing temperature, indicating that higher temperatures are unfavourable for MPB adsorption by the composite (6, 9, 36). The energy of adsorption (E) obtained from the Dubinin-Radushkevich plots is 1.118, 1.000, and 0.845 kJ $mol^{-1}$ at 303, 308, and 313 K, respectively. This implies that physisorption dominates the adsorption of MPB by AgNPs/Nanobiochar/Co-MOF composite as E < 8 $KJmol^{-1}$ at all observed temperatures (21, 38).

## Adsorption kinetics

The kinetics and mechanism of the adsorption process of MPB on AgNPs/Nanobiochar/Co-MOF composite carried out at 303 K, pH = 6 using 70 $mgL^{-1}$ of MPB and 0.5 g of composite, were described by pseudo-first-order (PFO) kinetics, pseudo-second-order kinetics (PSO), Elovich, and Intraparticle diffusion. The suitability of the kinetic models was determined by the correlation coefficient ($R^2$) of the plot, proximity of the $qe_{experimental}$ and $qe_{calculated}$, and RMSE. The plots of PFO, PSO, Elovich and Intraparticle diffusion are presented in Fig. 29, 30, 31 and 32, respectively. The parameters of the different models are compiled in Table 4. The PSO offers the best fit for the adsorption process due to agreement between the experimental and calculated $q_e$ value (Table 4), a higher correlation coefficient value of the PSO plot, and the lowest RMSE. The higher value of α over β in the Elovich model (Fig. 31 and Table 4) elicits the irreversibility and spontaneity of the adsorption process (21). The adsorption process of MPB on AgNPs/Nanobiochar/Co-MOF composite was influenced by adsorption, intramolecular, and intraparticle diffusion in the rate-determining step, as revealed by the non-intersection of the intraparticle diffusion plot with the origin (Fig. 32). The fitness of the adsorption process to the PSO kinetic suggests that the process of adsorption is through chemisorption (8, 31).



**DOI:** https://doi.org/10.53704/fujnas.v15i2.1330

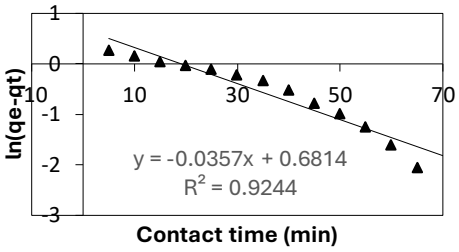


**Figure 29. Pseudo first order kinetic (PFO) model of methylparaben (MPB) adsorption on AgNPs/Nanobiochar/Co-MOF composite (Volume = 25 ml, dose = 0.5 g, Temperature = 303 K, pH = 6, agitation speed = 150 rpm, time of agitation = 5 – 100 min and concentration = 70 mgL$^{-1}$).**

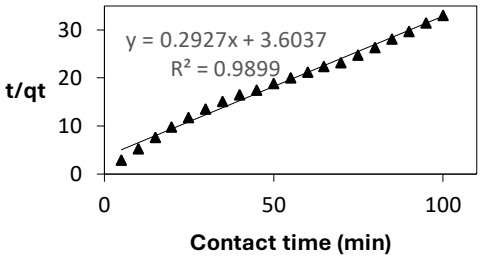


**Figure 30. Pseudo-second order (PSO) model of methylparaben (MPB) adsorption on AgNPs/Nanobiochar/Co-MOF composite (Volume = 25 ml, dose = 0.5 g, Temperature = 303 K, pH = 6, agitation speed = 150 rpm, time of agitation = 5 – 100 min and concentration = 70 mgL$^{-1}$).**

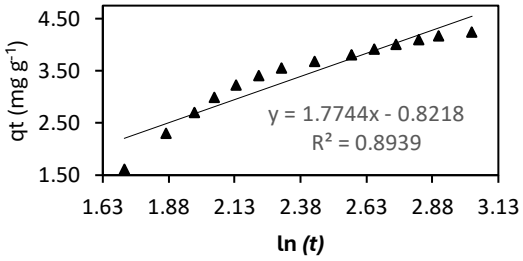


**Figure 31. Elovich model of methylparaben (MPB) adsorption on AgNPs/Nanobiochar/Co-MOF composite (Volume = 25 ml, dose = 0.5 g, Temperature = 303 K, pH = 6, agitation speed = 150 rpm, time of agitation = 5 – 100 min and concentration = 70 mgL$^{-1}$).**

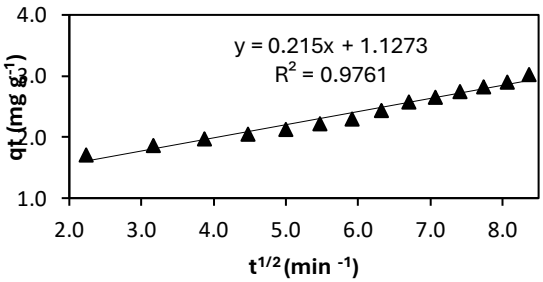


**Figure 32. Intra-particle diffusion model of methylparaben (MPB) adsorption on AgNPs/Nanobiochar/Co-MOF composite (Volume = 25 ml, dose = 0.5 g, Temperature = 303 K, pH = 6, agitation speed = 150 rpm, time of agitation = 5 – 100 min and concentration = 70 mgL$^{-1}$).**

## Adsorption thermodynamics

The thermodynamic parameters involved in the adsorption process are obtained from van't Hoff's plot (Fig. 33), and the values are presented in Table 5. The negative value of ($\Delta H^o$) and ($\Delta S^o$) implies that the adsorption process was exothermic. The degree of randomness at the MPB/ AgNPs/Nanobiochar/Co-MOF composite interface decreased. The negative value of ($\Delta G^o$) at all temperatures showed that the adsorption process was spontaneous. The values of ($\Delta H° = 20.72$ kJ mol$^{-1}$) imply that the adsorption process was controlled by physisorption as $\Delta H° < 40$ kJ mol$^{-1}$ (37).

## Desorption/ reusability

In a bid to ascertain the reusability of AgNPs/Nanobiochar/Co-MOF composite, the adsorption/desorption experiment of AgNPs/Nanobiochar/Co-MOF composite/MPB was repeated five times using distilled water and 0.1 M NaOH. The desorption study results are shown in Fig. 34. The results indicate that the AgNPs/Nanobiochar/Co-MOF composite was reusable after several adsorption/desorption cycles, although the removal efficiency decreased with each cycle. The removal percentage of MPB by AgNPs/Nanobiochar/Co-MOF composites reduced from 90.65 to 49.86 % after five cycles (Fig. 34). The percentage removal of 49.86 % after five adsorption cycles reported in this study is comparatively lower than the removal percentage after the fifth adsorption cycle reported by other authors.

## Density functional theory (DFT) investigation of MPB adsorption on AgNPs/Nanobiochar/Co-MOF composite

### Geometry and reactivity of AgNPs/Nanobiochar/Co-MOF composite

The structures of Co-MOF and the AgNPs/Nanobiochar/Co-MOF composite (Fig. 35) were optimised without geometric constraints using a density functional approach; the relevant parameters obtained from the optimisation are listed in Tables 6 and 7. The rhombic geometry used in the simulation of silver is consistent with the stable configuration reported for silver nanoparticles in the literature (39).

Notable distinctions were observed in the geometry of the Co-MOF and AgNPs/Nanobiochar/Co-MOF composite. The attachment of Ag to the 2-methylimidazole ligand led



DOI: https://doi.org/10.53704/fujnas.v15i2.1330

**Table 3: Comparison of monolayer adsorption capacity of AgNPs/Nanobiochar/Co-MOF composite with other adsorbents for methylparaben (MPB) removal from aqueous solution**

| Adsorbent | Adsorbate | $q_{max}$ (mg $g^{-1}$) | References |
|---|---|---|---|
| Biobased carbon material | Methylparaben | 415.2 | (48) |
| Biochar-$CoFe_2O_4$ nanocomposite | Methylparaben | 166.67 | (35) |
| Commercial activated carbon | Methylparaben | 95.24 | (36) |
| Tyre activated carbon-chitosan composite | Methylparaben | 85.9 | (6) |
| amino-functionalized magnetic nanoparticles | Methylparaben | 75 | (8) |
| Pistachio hull derived activated carbon | Methylparaben | 55 | (5) |
| **AgNPs/Nanobiochar/Co-MOF composite** | **Methylparaben** | **45.19** | **This Study** |
| Laccase biocomposite | Methylparaben | 39.85 | (50) |
| Activated olive stones | Methylparaben | 27.86 | (36) |
| Calcined Mg–Al LDH | Methylparaben | 20.99 | (51) |
| Modified cellulose | Methylparaben | 9.58 | (12) |
| *Albizia lebbeck* leaves- AgNPs | Methylparaben | 6.7 | (49) |

**Table 4: Adsorption kinetics parameter of methylparaben (MPB) adsorption on AgNPs/Nanobiochar/Co-MOF composite**

| | | |
|---|---|---|
| $qe_{experiment}$ (mg $g^{-1}$) | | 3.03 |
| Pseudo-first order | $qe_{calculated}$ (mg $g^{-1}$) | 1.98 |
| | $K_1$ ($min^{-1}$) | 0.036 |
| | $R^2$ | 0.8319 |
| | *RMSE* | 1.171 |
| Pseudo-second order | $qe_{calculated}$ (mg $g^{-1}$) | 3.17 |
| | $K_2$ ($gmg^{-1}min^{-1}$) | 0.028 |
| | $R^2$ | 0.993 |
| | *RMSE* | 0.787 |
| Elovich | α (g $mg^{-1}$) | 1.117 |
| | β (mg $g^{-1}$ $min^{-1}$) | 0.564 |
| | $R^2$ | 0.8939 |
| Intra-particle diffusion | $K_{diff}$ ($mgg^{-1}min^{-1/2}$) | 0.215 |
| | C (mg $g^{-1}$) | 1.127 |

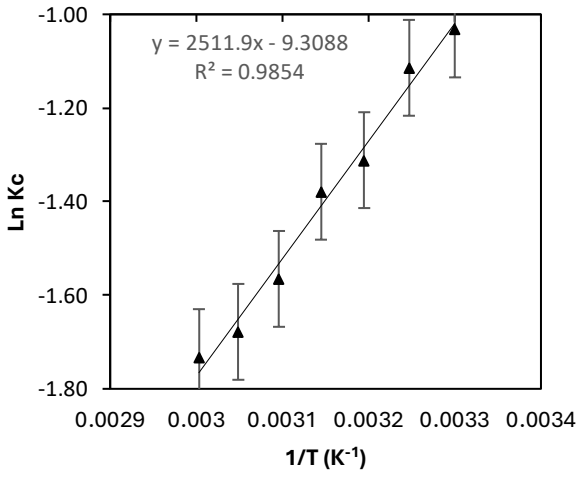


**Figure 33. Van't Hoff thermodynamic model for adsorption of Methylparaben (MPB) by AgNPs/Nanobiochar/Co-MOF composite (Volume = 25 ml, dose = 0.5 g, temperature = 303 K, pH = 6, agitation speed = 150 rpm, time of agitation = 30 min and concentration = 70 mg $L^{-1}$).**

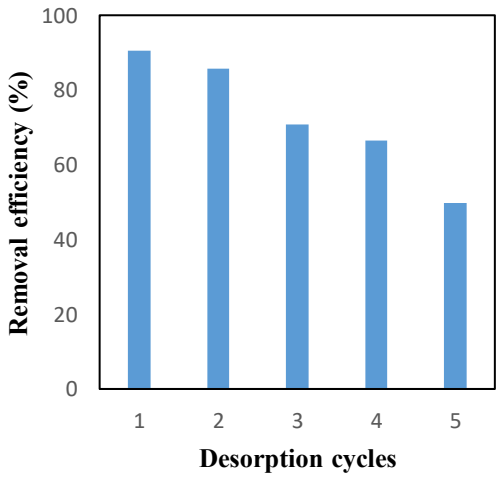


**Figure 34. Removal efficiency of MPB in 5 adsorption–desorption cycles.**



**DOI:** https://doi.org/10.53704/fujnas.v15i2.1330

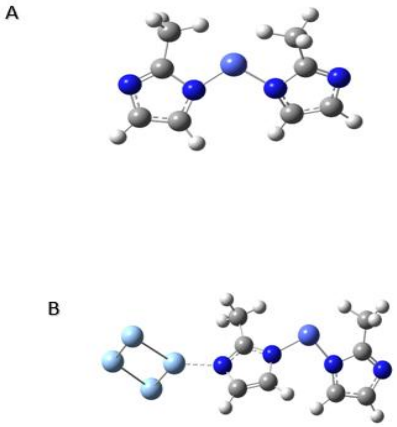


**Figure 35. Optimized structure of Co-MOF (A) and AgNPs/Nanobiochar/Co-MOF composite (B) calculated at B3LYP/def2svp, gd3**

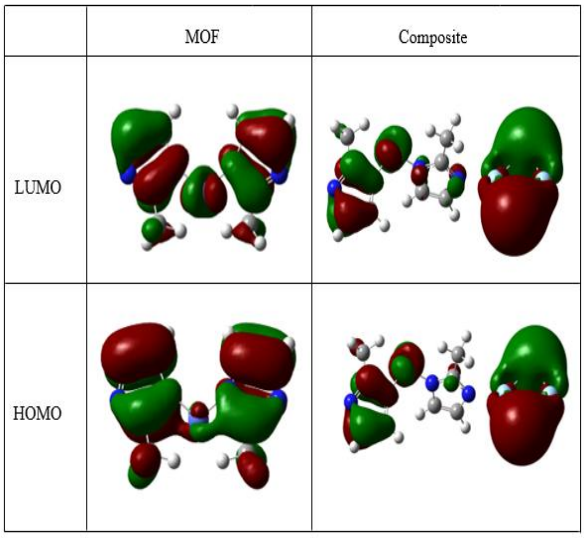


**Figure 36. Frontier molecular orbital for the Co-MOF and AgNPs/Nanobiochar/Co-MOF composite calculated at B3LYP/def2svp, gd3**

to an increase in the bond length of $Co_1$-$N_2$ and $Co_1$-$N_{13}$ in the composite, and the angle of tilt around the Co metal Centre linkage in the optimised structure of the composite. In addition, the introduction of silver nanoparticles led to cleavage and rearrangement of bonds in the composite, delocalisation of electrons, and destruction of the double bond at N2-C3 and C3=N4 in the optimised structure of the composite (Table 6). The Frontier molecular orbital energies (HOMO and LUMO) (Fig. 36) of the composite were greater than those of the parent compound (MOF), indicating the increased reactivity of the composite over MOF. The Molecular electrostatic potential (Fig. 37) indicates a reduction in electron density distribution on the 2-methylimidazole ligand of the composite compared to the MOF.

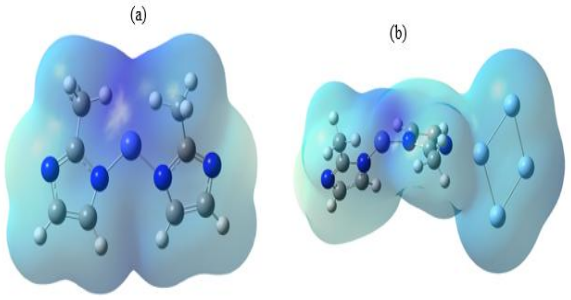


**Figure 37. Molecular electrostatic potential for the molecules; (a) Co-MOF, (b) AgNPs/Nanobiochar/Co-MOF Composite, calculated at B3LYP/def2svp, gd3**

## Molecular Docking

To understand the adsorption mechanism of MPB –AgNPs/Nanobiochar/Co-MOF composite, calculations are undertaken via Density Functional Theory (DFT) to obtain the binding energy, which could be correlated to the strength of interaction between the composite and methylparaben (MPB). The results presented in (Fig. 38) show that the adsorption of MPB molecules could result from its interaction with the Co metal centre of the composite (complex (a) and (b)) and the uncoordinated N atom of the imidazole ring (complex (c)).

The negative values of binding energies in complex (a) and (b) indicate the strength of the interactions, and affirm the exergonic process of adsorption involving virtually electrostatic attraction, resulting from the transfer of an electron from MPB to the composite, as indicated by the Mulliken

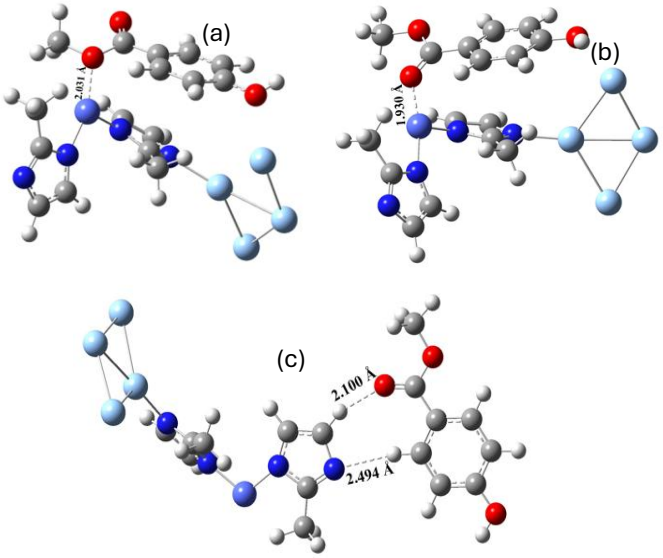


**Figure 38. The optimised structures for the possible interactions between the AgNPs/Nanobiochar/Co-MOF composite and methylparaben (MPB) were calculated at B3LYP/ def2svp, gd3.**



DOI: https://doi.org/10.53704/fujnas.v15i2.1330

**Table 5:** Thermodynamic parameters for MPB – AgNPs/Nanobiochar/Co-MOF composite adsorption process

| | Methylparaben | | | |
|---|---|---|---|---|
| Temperature (K) | $\Delta G^o$ (kJ mol$^{-1}$) | $\Delta H^o$ (kJ mol$^{-1}$) | $\Delta S^o$ (J mol$^{-1}$ K$^{-1}$) | $R^2$ |
| 303 | -16.0 | | | 0.9854 |
| 308 | -15.9 | | | |
| 313 | -15.8 | | | |
| 318 | -15.7 | -20.72 | -15.714 | |
| 323 | -15.6 | | | |
| 328 | -15.5 | | | |
| 333 | -15.4 | | | |

**Table 6: Geometric parameters of Co-MOF and AgNPs/Nanobiochar/Co-MOF composite**

| Parameters | MOF | Composite |
|---|---|---|
| Bond length (Å) | | |
| $Co_1$-$N_2$ | 1.767 | 1.833 |
| $N_2$-$C_3$ | 1.418 | 1.354 |
| $C_3$-$N_4$ | 1.300 | 1.340 |
| $N_4$-$C_5$ | 1.374 | 1.387 |
| $C_5$-$C_6$ | 1.407 | 1.369 |
| $C_6$-$N_2$ | 1.345 | 1.386 |
| $C_3$-$C_7$ | 1.492 | 1.494 |
| $C_7$-$H_8$ | 1.126 | 1.102 |
| $C_7$-$H_9$ | 1.100 | 1.103 |
| $C_7$-$H_{10}$ | 1.103 | 1.101 |
| $C_5$-$H_{11}$ | 1.091 | 1.088 |
| $C_6$-$H_{12}$ | 1.087 | 1.087 |
| $Co_1$-$N_{13}$ | 1.767 | 1.786 |
| $N_{13}$-$C_{14}$ | 1.418 | 1.391 |
| $C_{14}$-$N_{15}$ | 1.301 | 1.308 |
| $N_{15}$-$C_{16}$ | 1.375 | 1.377 |
| $C_{16}$-$C_{17}$ | 1.408 | 1.398 |
| $C_{17}$-$N_{13}$ | 1.345 | 1.357 |
| $C_{14}$-$C_{18}$ | 1.492 | 1.496 |
| $C_{18}$-$H_{19}$ | 1.103 | 1.102 |
| $C_{18}$-$H_{20}$ | 1.126 | 1.126 |
| $C_{18}$-$H_{21}$ | 1.099 | 1.100 |
| $C_{16}$-$H_{22}$ | 1.091 | 1.109 |
| $C_{17}$-$H_{23}$ | 1.087 | 1.087 |
| $N_4$-$Ag_{24}$ | - | 2.153 |
| $Ag_{24}$-$Ag_{25}$ | - | 2.835 |
| $Ag_{25}$-$Ag_{26}$ | - | 2.764 |
| $Ag_{27}$-$Ag_{27}$ | - | 2.768 |
| Bond angle (°) | | |
| $N_2$-$Co_1$-$N_{13}$ | 107.8 | 104.0 |
| $Co_1$-$N_2$-$C_3$ | 103.9 | 128.4 |
| $Co_1$-$N_{13}$-$C_{14}$ | 104 | 106.8 |
| $Co_1$-$N_2$-$C_6$ | 147.5 | 124.7 |
| $Co_1$-$N_{13}$-$C_{17}$ | 147.5 | 147.0 |
| Dihedral angle (°) | | |
| $N_2$-$Co_1$-$N_{13}$-$C_{17}$ | 26.4 | 9.8 |
| $N_{13}$-$Co_1$-$N_2$-$C_6$ | 26.6 | 48.5 |



**DOI:** https://doi.org/10.53704/fujnas.v15i2.1330

**Table 7: Reactivity parameters Co-MOF and AgNPs/Nanobiochar/Co-MOF composite in eV**

| Compound | $E_{HOMO}$ | $E_{LUMO}$ | $\Delta E_{HOMO-LUMO}$ | IP | EA | χ |
|---|---|---|---|---|---|---|
| MOF | -10.45 | -9.09 | 1.36 | 10.45 | 9.09 | 0.68 |
| Composite | -7.98 | -7.56 | 0.42 | 7.98 | 7.56 | 0.21 |

**Table 8: Probable modes of interactions between AgNPs/Nanobiochar/Co-MOF composite and substrates (methylparaben), and the interaction descriptors, calculated at B3LYP/ def2svp, gd3.**

| Complex | Type of interactions | Binding energy (BE) (kcal/mol) | Change in Gibbs free energy ΔG (kcal/mol) | Interatomic distance (Å) | Electrons transferred to the composite (Mulliken) |
|---|---|---|---|---|---|
| Complex (a) | $CH_3O$---Co | -42.416 | -25.773 | 2.031 | -0.287 |
| Complex (b) | C=O---Co | -53.751 | -37.481 | 1.930 | -0.329 |
| Complex (c) | C=O---H-Imz, -N---H-Ph | -7.847 | 2.00 | 2.100, 2.494 | -0.039 |

charge analysis reported in Table 8. The negative values computed for the ΔGs attest to the feasibility of the adsorption processes for the interaction in complex (a) and (b) (Table 8). However, the mode of interaction in complex (b) seems to be more probable for the adsorption than that of complex (a), due to its greater strength of interaction (binding energy), greater electron transfer, and lower ΔG predicted for the interaction (33, 43). The favourability of the interaction in complex (b) for the adsorption could be attributed to the enhancement in the electron density of the carbonyl (C=O) functional group due to the sandwich arrangement in which it receives electrons from the phenolic ring via mesomeric effect and the methoxy moiety through inductive effect (40, 41). This eventually translated to the greater interaction predicted for the complex (b) as a larger quantity of electrons would be available for transfer to the Co metal centre than the complex (a), where the electron density on the $OCH_3$ would have been decreased inductively.

In complex (c), the positive value computed for the ΔG of hydrogen bonding interaction (Fig. 38) signals an endergonic process, which normally requires energy to occur. The predicted C=O---H-Imz interatomic distance (2.10 Å) and the strength of interaction (-7.85 kcal/mol) suggest a strong hydrogen bonding interaction (42). In a nutshell, it is safe to assume that the adsorption of MPB by the AgNPs/Nanobiochar/Co-MOF composite was brought about mainly by the interaction of the MPB with the metal centre of the composite, and a possible contribution from hydrogen bonding at elevated temperature.

## Conclusion

A nano-porous composite of Nanobiochar, nanoparticles, and cobalt metal organic framework was successfully prepared, as demonstrated by the FTIR, EDX, and BET results. The pH point of zero charge of the adsorbent and the pH of maximum adsorption of MPB were observed at 8.8 and 6, respectively. The Freundlich isotherm accurately described the adsorption process, as indicated by a higher correlation coefficient. Data obtained for the thermodynamic study indicate that the adsorption process was feasible, spontaneous, and exothermic, with a decreased degree of disorderliness at the MPB/composite interface. The binding of MPB to AgNPs/Nanobiochar/Co-MOF composites is multilayered and through physisorption as dictated by parameters of the Freundlich isotherm, Dubinin-Radushkevich, and Van't Hoff's thermodynamic plot. Molecular docking study affirms the feasibility of the adsorption process, as evidenced by the binding energy and the negative Gibbs free energy change. The computational study revealed that the cobalt metal centre of the composite was the point of interaction with methylparaben (MPB), and that the composite exhibited increased reactivity over MOF.

## Conflict of interests

The authors declare no competing interests.

### References

1. Adeola AO, Oyedotun KO, Waleng NJ, Mamba NB, Nomngongo PN. Onion skin–derived sorbent for the sequestration of methylparaben in contaminated aqueous medium. *Biomass Convers Biorefin*. 2023. doi:10.1007/s13399-023-04332-4.
2. De Oliveira FF, Moura KO, Costa LS, Vidal CB, Loiola AR, Do Nascimento RD. Reactive adsorption of parabens on synthesized micro- and mesoporous silica from coal fly ash:

pH effect on the modification process. *ACS Omega*. 2020;5:3346–3357. doi:10.1021/acsomega.9b03537.
3. Bernal-Romero del Hombre Bueno M, Boluda-Botella N, Daniel PR. Removal of emerging pollutants in water treatment plants: adsorption of methyl and propylparaben onto powdered activated carbon. *Adsorption*. 2019. doi:10.1007/s10450-019-00120-7.
4. Bolujoko NB, Emmanuel IU, Moses OA, Aemere O, Olumuyiwa OO, Martins OO, et al. Toxicity and removal of parabens from water: a critical review. *Sci Total Environ*. 2021. doi:10.1016/j.scitotenv.2021.148092.
5. Nodeh HM, Hassan S, Sahar A, Amirarshia T, Ali TR. Activated carbon derived from pistachio hull biomass for the effective removal of parabens from aqueous solutions: isotherms, kinetics, and free energy studies. *Desalin Water Treat*. 2020. doi:10.5004/dwt.2020.25985.
6. Mashile GP, Anele M, Azile N, Dimpea KM, Philiswa NN. Recyclable magnetic waste tyre activated carbon–chitosan composite as an effective adsorbent for rapid and simultaneous removal of methylparaben and propylparaben from aqueous solution and wastewater. *J Water Process Eng*. 2020. doi:10.1016/j.jwpe.2019.101011.
7. Sheikhmohammadi A, Safari M, Alinejad A, Esrafili A, Nourmoradi H, Asgari E. $Fe_3O_4$@$SiO_2$ nanoparticles functionalized with 3-aminopropyltriethoxysilane as an efficient sorbent for adsorption of ethylparaben from wastewater. *J Environ Chem Eng*. 2019. doi:10.1016/j.jece.2019.103315.
8. Mohammadi F, Ali E, Hamid RS, Mohammad B, Majid K, Esrafil A, et al. Evaluation of adsorption and removal of methylparaben from aqueous solutions using amino-functionalized magnetic nanoparticles. *Desalin Water Treat*. 2018. doi:10.5004/dwt.2018.21781.
9. Bernal V, Giraldo L, Moreno-Piraján JC. Physicochemical parameters of methylparaben adsorption from aqueous solution onto activated carbon and their relationship with surface chemistry. *ACS Omega*. 2021;6:8797–8807. doi:10.1021/acsomega.0c05368.
10. Mejías C, Martín J, Santos JL, Aparicio I, Alonso E. Role of polyamide microplastics as vector of parabens in the environment: an adsorption study. *Environ Technol Innov*. 2023;32:103276. doi:10.1016/j.eti.2023.103276.
11. Zhou X, Zhou JY, Liu Y, He J, Ren J. Adsorption of endocrine-disrupting ethylparaben from aqueous solution by chemically activated biochar from oil palm fibre. *Sep Sci Technol*. 2018. doi:10.1080/01496395.2018.1520723.
12. Correa-Navarro YM, Rivera-Giraldo JD, Cardona-Castaño JA. Modified cellulose for adsorption of methylparaben and butylparaben from aqueous solution. *ACS Omega*. 2024;9:30224–30233. doi:10.1021/acsomega.3c10304.
13. Eltaweil AS, Mamdouh IM, Abd El-Monaem EM, El-Subruiti GM. Highly efficient removal of methylene blue and $Cu^{2+}$ onto UiO-66 MOF/graphene oxide incorporated sodium alginate beads. *ACS Omega*. 2021;6:23528–23541. doi:10.1021/acsomega.1c03479.
14. Roy D, Neogi S, De S. Adsorptive removal of heavy metals from battery industry effluent using MOF incorporated polymeric beads: a combined experimental and modeling approach. *J Hazard Mater*. 2020.
15. Hoseinzadeh H, Hayati B, Ghaheh FS, Seifpanahi-Shabani K, Mahmoodi NM. Development of room temperature synthesized and functionalized metal-organic framework/graphene oxide composite and pollutant adsorption ability. *Mater Res Bull*. 2021. doi:10.1016/j.materresbull.2021.111408.
16. Xu K, Bi Y, Wei Y, Li X, Liu Y, Lin Y, Wang C, Hu G, Liu Q, Zhang Y. Facile in-situ growth of ZIF-67 nanoparticles and polymerization on chitosan aerogel spheres for tetracycline adsorption. *J Solid State Chem*. 2024. doi:10.1016/j.jssc.2023.124442.
17. Lin KYA, Chang HA. Ultra-high adsorption capacity of ZIF-67 for removal of malachite green from water. *Chemosphere*. 2015. doi:10.1016/j.chemosphere.2015.01.004.
18. Pouramini Z, Mousavi SM, Babapoor A, Hashemi SA, Lai CW, Mazaheri Y, et al. Effect of metal atom in ZIF-8 and ZIF-67 for removal of dyes and antibiotics from wastewater: a review. *Catalysts*. 2023;13:155. doi:10.3390/catal13010155.
19. Zhong G, Liu D, Zhang J. The application of ZIF-67 and its derivatives: adsorption, separation, electrochemistry and catalysts. *J Mater Chem A*. 2018. doi:10.1039/c7ta08268a.
20. Azeez L, Adebisi SA, Adetoro RO, Oyedeji AO, Agbaje WB, Olabode OA. Foliar application of silver nanoparticles in *Abelmoschus esculentus*. *Int J Phytoremediation*. 2021. doi:10.1080/15226514.2021.1949578.
21. Azeez L, Adebisi SA, Adejumo AL, Busari HK, Aremu HK, Olabode OA, et al. Adsorptive properties of silver nanoparticle-functionalized hydroxyapatite. *Inorg Chem Commun*. 2022. doi:10.1016/j.inoche.2022.109655.
22. Wei S, Mengbo Z, Xingjun F, Jianzhong S, Ping'an P, Kaiming L, et al. Influence of pyrolysis temperature and feedstock on carbon fractions of biochar. *Chemosphere*. 2019. doi:10.1016/j.chemosphere.2018.11.177.
23. Al Murisi M, Al-Asheh S, Abdelkareem M, Aidan A, Elsaid K, Abdul Ghani O. In situ growth of ZIF-67 on carbon cloth for oxygen reduction reactions. *ACS Omega*. 2023. doi:10.1021/acsomega.3c02544.
24. Davoodi M, Davar F, Rezayat MR, Jafari MT, Bazarganipour M, Shalan AE. Synthesis and characterization of ZIF-67@$MgAl_2O_4$ nanocomposite and its adsorption behavior. *RSC Adv*. 2021. doi:10.1039/d1ra01056e.
25. Kohantorabi M, Stefanos G, Gholamreza M, Michael B, Mohammad RG, Cesar P. Ag/ZIF-67@GO nanocomposite with peroxymonosulfate activation efficacy. *J Hazard Mater*. 2021. doi:10.1016/j.jhazmat.2021.125308.
26. Azeez L, Adetoro RO, Busari HK, Aremu HK, Adeleke JT, Adewinbi S, et al. AgNPs–$TiO_2$NPs doped hydroxyapatite for removal of pharmaceuticals. *Int J Environ Anal Chem*. 2022. doi:10.1080/03067319.2022.2106434.
27. Frisch MJ, Trucks GW, et al. Gaussian 09, Revision A.02. Wallingford (CT): Gaussian Inc.; 2016.
28. Weigend F, Ahlrichs R. Balanced basis sets for H to Rn: design and accuracy. *Phys Chem Chem Phys*. 2005;7:3297–3305.
29. Weigend F. Accurate Coulomb-fitting basis sets for H to Rn. *Phys Chem Chem Phys*. 2006;8:1057–1065.
30. Li P, Zhao T, Zhao Z, Tang H, Feng W, Zhang Z. Biochar from herbal residues for dye adsorption. *ACS Omega*. 2023;8:4813–4825. doi:10.1021/acsomega.2c06968.
31. Azeez L, Adefunke O, Oyedeji AO, Agbaogun BK, Busari HK, Adejumo AL, et al. Removal of rhodamine B and metronidazole using mesoporous biochar. *Water Pract Technol*. 2024;19:730. doi:10.2166/wpt.2024.049.
32. Chen G, He S, Shi G, Ma Y, Ruan C, Jin X, et al. In-situ immobilization of ZIF-67 on wood aerogel. *Chem Eng J*. 2021. doi:10.1016/j.cej.2021.130184.

33. Azeez L, Adeleke AE, Popoola SA, Busari HK, Agbaje WB, Ojewuyi SS, et al. Dye degradation and molecular docking of $TiO_2$ nanoparticles. *Inorg Chem Commun*. 2023;153:110873. doi:10.1016/j.inoche.2023.110873.
34. Hidayat ARP, Zulfa LL, Widyanto AR, Abdullah R, Kusumawati Y, Ediati R. Selective adsorption of dyes on mesoporous UiO-66. *RSC Adv*. 2023;13:12320–12343. doi:10.1039/D2RA06947D.
35. Fito J, Nkambule TTI. Biochar-$CoFe_2O_4$ nanocomposite for methylparaben adsorption. *Environ Monit Assess*. 2023;195:241. doi:10.1007/s10661-022-10819-w.
36. León G, Hidalgo AM, Martínez A, Guzmán MA, Miguel B. Methylparaben adsorption onto activated carbon and olive stones. *Appl Sci*. 2023;13:9147. doi:10.3390/app13169147.
37. Yusoff MM, Yahaya N, Saleh NM, Raoov M. Removal of parabens using ionic liquid-loaded adsorbent. *RSC Adv*. 2018. doi:10.1039/c8ra03408g.
38. Sulaiman WK, Azeez L, Adebisi SA, Wahab OO, Agbaogun BK. Zero-valent iron nanoparticles for bisphenol A removal. *Water Pract Technol*. 2024;19:3416. doi:10.2166/wpt.2024.209.
39. Onawole AT, Popoola SA, Saleh TA, Al-Saadi AA. Silver-loaded graphene for clotrimazole detection. *Spectrochim Acta A Mol Biomol Spectrosc*. 2018.
40. McMurry JE. *Organic Chemistry*. 3rd ed. Belmont (CA): Wadsworth; 1992.
41. Popoola SA, Al-Harbi MHM, Al-Rashidi AH. DFT evaluation of substituted bipyridine derivatives. *J Taibah Univ Sci*. 2020;14:1527–1537.
42. Macleod JM, Rosei F. Directed assembly of nanostructures. In: *Comprehensive Nanoscience and Technology*. Elsevier; 2011. p. 13–61.
43. Abdelbassit MS, Popoola SA, Saleh TA. DFT and kinetic evaluation of chloromethane removal. *Arab J Sci Eng*. 2020;45:4705–4716.
44. Guha AK, Das C, Phukan AK. Heterocyclic carbenes of diverse flexibility. *J Organomet Chem*. 2011;696:586–593.
45. Grimme S, Antony J, Ehrlich S. Accurate parametrization of DFT-D dispersion correction. *J Chem Phys*. 2010;132:154104.
46. Lee C, Yang W, Parr RG. Development of the Colle-Salvetti correlation-energy formula. *Phys Rev B*. 1988;37:785–789.
47. Becke AD. Density-functional thermochemistry III: role of exact exchange. *J Chem Phys*. 1993;98:5648–5652.